THE AMERICAN SOCIETY OF MECHANICAL ENGINEERS
345 E. 47th St., New York, N.Y. 10017

95-GT-463

BOUNDARY LAYER DEVELOPMENT IN AXIAL COMPRESSORS AND TURBINES PART 3 OF 4: LP TURBINES

David E. Halstead
GE Aircraft Engines
Cincinnati, OH

David C. Wisler
GE Aircraft Engines
Cincinnati, OH

Theodore H. Okiishi
Iowa State University
Ames, IA

Gregory J. Walker
University of Tasmania
Hobart, Australia

Howard P. Hodson
University of Cambridge
Cambridge, UK

Hyoun-Woo Shin
GE Aircraft Engines
Cincinnati, OH

ABSTRACT

This is Part Three of a four-part paper. It begins with Section 11.0 and continues to describe the comprehensive experiments and computational analyses that have led to a detailed picture of boundary layer development on airfoil surfaces in multistage turbomachinery.

In this part, we present the experimental evidence that we used to construct the composite picture for LP turbines that was given in the discussion in Section 5.0 of Part 1. We present and interpret the data from the surface hot-film gauges and the boundary layer surveys for the baseline operating condition. We then show how this picture changes with variations in Reynolds number, airfoil loading and nozzle-nozzle clocking.

11.0 FORMAT FOR DATA PRESENTATION AND INTERPRETATION

This section describes the format we use to present our results and the techniques we use to identify transition.

11.1 Space-Time (s-t) Diagrams and Line Plots

The time history of the developing boundary layer is described by s-t diagrams which show contour plots of ensemble-averaged random unsteadiness and skew measured with surface hot-film gauges. Airfoil surface length is plotted along the abscissa and time, in units of wake passing period, is plotted along the ordinate. Examples are shown in Figs. 28a and b. The color red on the contour plots represents the highest values of the variable measured, and the color blue represents the lowest. There is a linear variation of ten equal increments (changes in color) between red and blue. Reference color legends are shown only in Fig. 28. For all other color contour plots, the highest value of the quantity (plotted in red) is given in the figure caption as Q_{10} and the lowest value (plotted in blue) as Q_0. The reader can refer to the reference color legends to decode the values the colors represent.

Important regions of the s-t diagram are identified by letters A, B, etc., and points of specific interest are identified by numbers 1, 2, etc. Trajectories W, X, Y and Z are drawn at selected percentages of the wake passing period. Trajectory W always extends along the wake-induced path.

Distributions of quasi wall shear stress, random unsteadiness and skew are also shown as line plots. Black lines through the black symbols on the plots denote the time-average of the data, as seen in Figs. 28c, d and e. Colored lines denote values along trajectories W, X, Y and Z. The dashed lines, shown for quasi wall shear stress only, denote the minimum and maximum values of the unsteady data. These dashed lines do not represent error bars.

11.2 Identifying Transition

In a manner identical to that for the compressor, we identify transition regions and infer values of intermittency from the variations in skew and random unsteadiness along the airfoil surface. Since skew provides a measure of the asymmetry in fluctuations of wall shear stress about the mean, its value is positive when the transitional flow is more laminar than turbulent. Its value is negative when the transitional flow is more turbulent than laminar. Therefore as shown in Fig. 12d of Part 2, skew is zero prior to transition onset (intermittency $\gamma = 0$), skew reaches a maximum positive value at $\gamma \approx 0.25$, skew is zero at the midpoint of transition $\gamma \approx 0.50$, skew is a negative maximum at $\gamma \approx 0.75$, and skew is zero when transition is complete, $\gamma = 1.0$. At the same time skew is varying in this manner, the random unsteadiness increases from a laminar level at $\gamma = 0$ to a peak value at $\gamma \approx 0.50$. It then decreases in

Presented at the International Gas Turbine and Aeroengine Congress & Exposition
Houston, Texas - June 5-8, 1995
This paper hs been accepted for publication in the Transactions of the ASME
Discussion of it will be accepted at ASME Headquarters until September 30, 1995

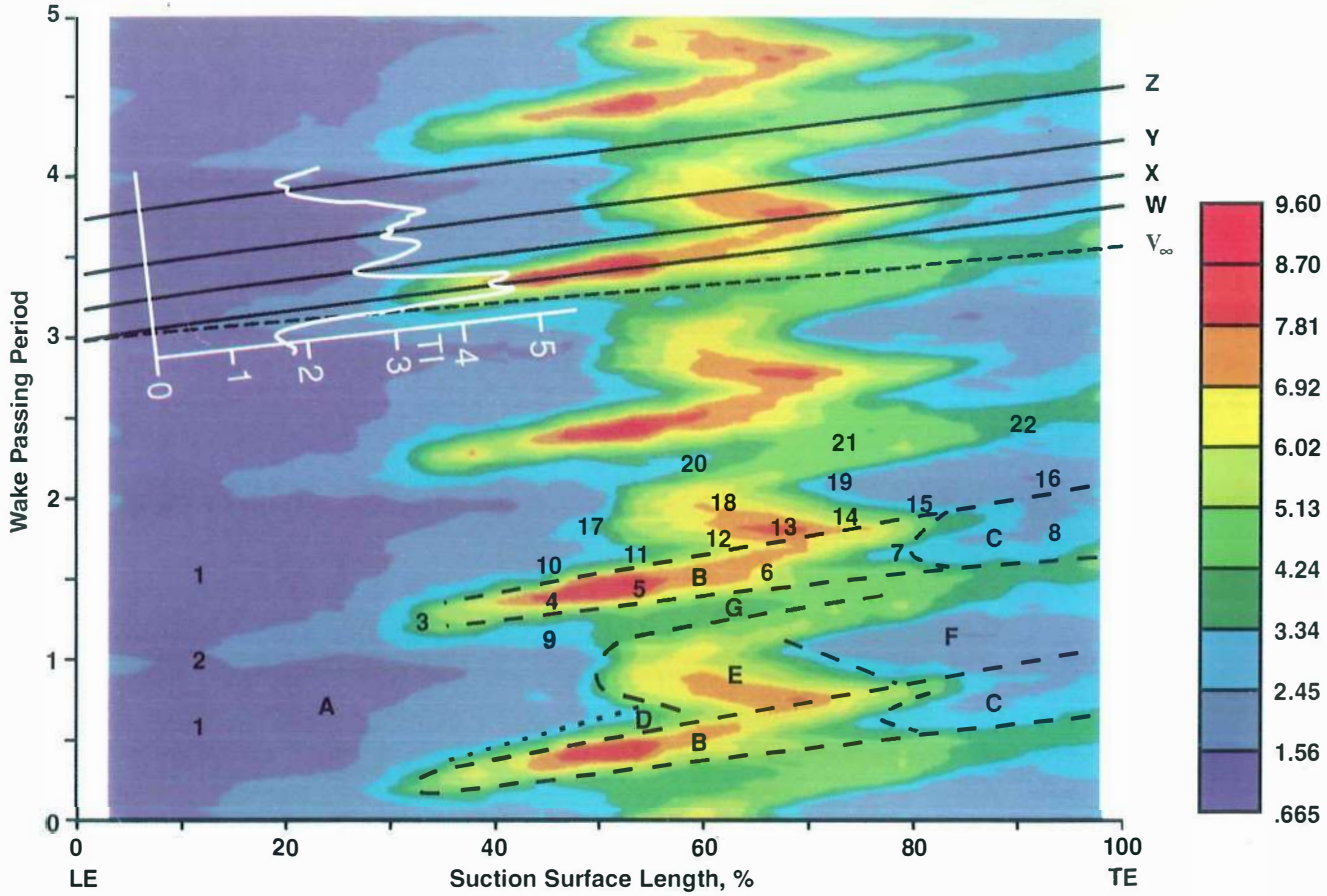

a) Random Unsteadiness $Q_0 = 0.67$, $Q_{10} = 9.60$

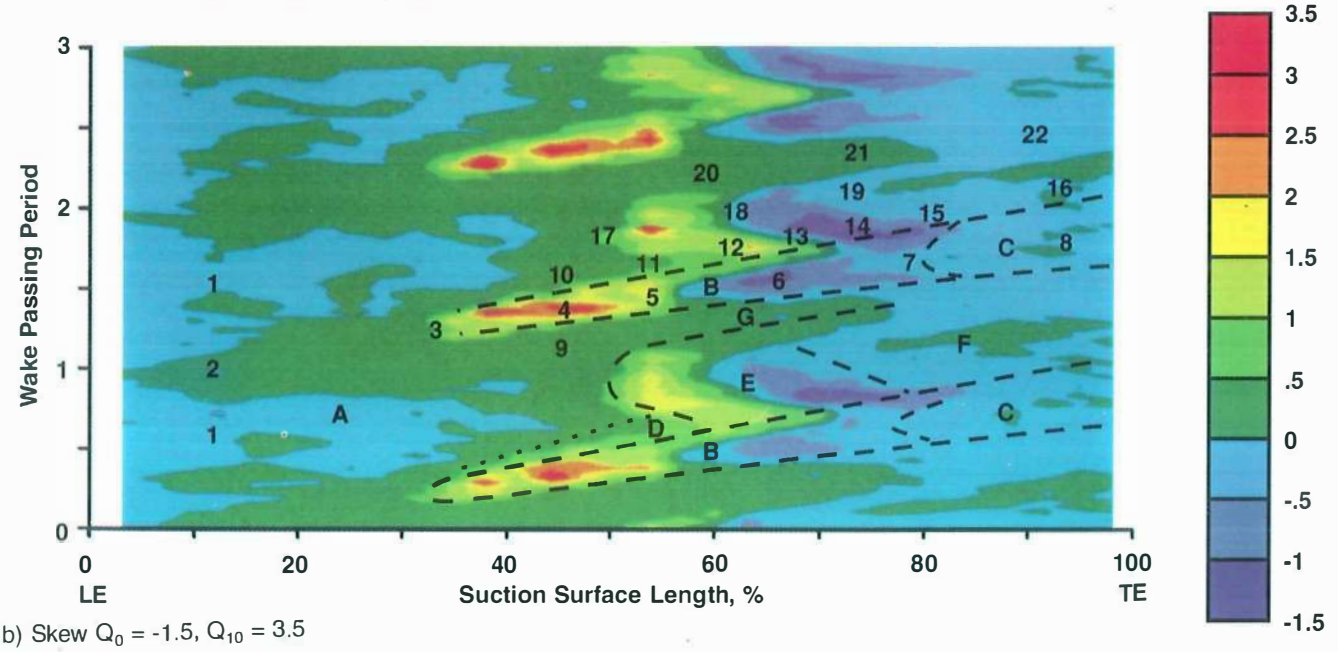

b) Skew $Q_0 = -1.5$, $Q_{10} = 3.5$

Fig. 28 Shear stress characteristics on suction surface of second stage nozzle N2, $\overline{Re} = 5.27 \times 10^5$, Turbine baseline test point 5A. a–b) s–t diagram, c–e) Trajectories W, X, Y, Z.

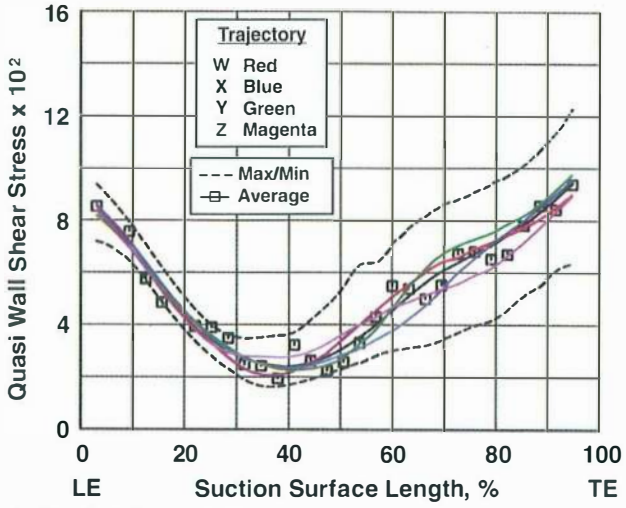

c) Quasi wall shear stress

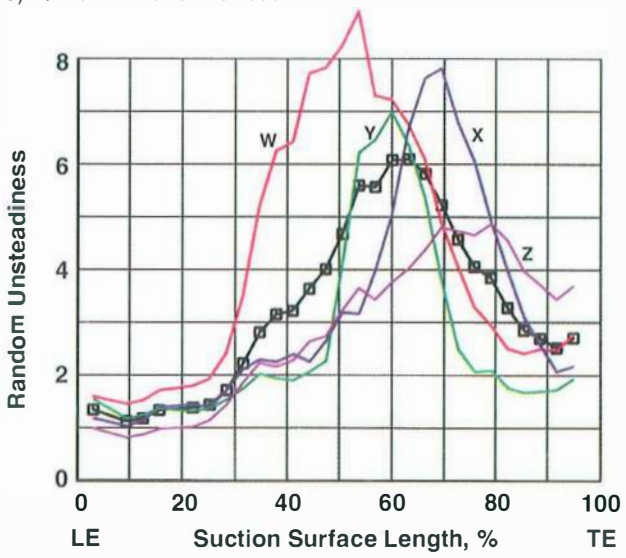

d) Random unsteadiness

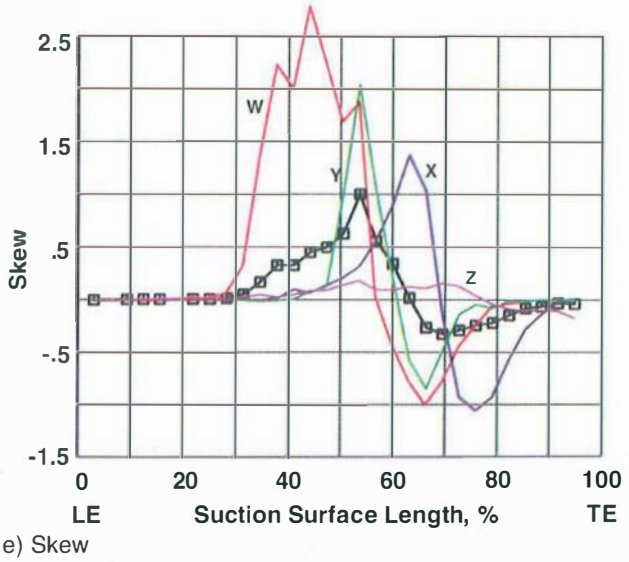

e) Skew

Fig. 28 Continued

value as transition is completed. Thus peak random unsteadiness occurs near zero skew and 50 percent intermittency.

Since it is easy to identify where intermittency is 0.75 from skew data, we have selected $\gamma = 0.75$ as a figure of merit for identifying the location where the wake-induced strips are capable of generating effective calmed regions. This provides consistency for comparison purposes.

12.0 BOUNDARY LAYER DEVELOPMENT FOR LP TURBINES

This section describes the development of the boundary layer along the embedded, second-stage nozzle airfoils of the LP turbine operating at baseline Test Point 5A. It provides the evidence for the composite picture for the turbine baseline given as Fig. 10b in the discussion in Section 5.0.

The relative clocking of nozzles N1 and N2 was selected to reduce the influence of the N1 wakes on the N2 boundary layers. For completeness, we have tabulated the locations of the laminar, transitional and turbulent regions for our turbine test cases in Table 6 at the end of Part 3.

The s-t diagrams, which show ensemble-average contour plots of random unsteadiness and skew, are presented in Figs. 28a and b for the suction surface of the nozzle. They are the turbine equivalent of the compressor results shown in Figs. 13a and b. Four trajectories, labeled W, X, Y and Z, are drawn at a speed of 0.7 V_∞, which is an average of the leading and trailing boundary speeds of a turbulent spot. These trajectories are not straight lines because the freestream velocity, V_∞, varies through the airfoil passage. Trajectory W is drawn through the wake-induced transitional/turbulent strips.

The distribution of turbulence intensity entering the nozzle row, shown as curve TI in Fig. 28a, has several distinct levels. Along the wake-induced path W, the turbulence intensity was about 4.6 percent. In the path between wakes, there were three levels of 2.7, 3.4 and 1.7 percent. These three levels result from the dispersion of the upstream nozzle wakes as will be shown in Section 15.0. Trajectories X, Y and Z, which are located in time at 20, 42 and 76 percent of the wake passing period following trajectory W, originate upstream along paths having the three respective levels of turbulence intensity.

The composite picture in Fig. 10b described the boundary layer as developing along two separate but coupled paths: the wake-induced path, which consists of regions A, B and C; and the path between wakes, which consists of regions A, D, E and F. These paths are examined below.

12.1 The Wake-Induced Path

As wakes from the upstream airfoil row convect along the downstream airfoil, a boundary layer on the downstream airfoil develops along a wake-induced path which lies approximately under the convecting wake. The wake-induced path begins in Figs. 28a and b at the leading edge, goes through points 2–3 in laminar region A and continues through both the

wake-induced transitional strip B and the wake-induced turbulent strip C to the trailing edge of the airfoil.

The Laminar Region (A). For the baseline test condition, a laminar boundary layer begins at the leading edge of the suction surface and continues downstream. This region is classified as laminar because it has low random unsteadiness and zero skew, seen respectively as the blue region A in Fig. 28a and the blue/green region A in Fig. 28b.

The portion of region A that interests us here occupies about 20–25 percent of the wake passing period. It lies approximately under the convecting wakes and extends from the leading edge along points 2–3 to about 32 percent SSL. Wake-induced trajectory W passes through this portion. Along 2–3, the laminar boundary layer is subjected to periodic and random unsteadiness from the passage of the rotor wakes. This appears as a slightly higher (but still low) level of random unsteadiness seen as the lighter blue area along points 2–3 in Fig. 28a. The skew along 2–3 is still near zero in Fig. 28b and wall shear stress is decreasing for trajectory W in Fig. 28c. This portion of region A constitutes the beginning of the wake-induced path.

Region A for the turbine has an even greater streamwise extent than that for the compressor in Fig. 13 of Part 2. This is due to the larger extent of the favorable pressure gradients existing along the turbine suction surface.

Wake-Induced Transitional Strip (B). There is a significant increase in random unsteadiness and skew along the path of the rotor wakes near 32 percent SSL at point 3 in Figs. 28a and b and along the red wake-induced trajectories W in Figs. 28d and e. These changes, which are in phase with the peak values of inlet turbulence intensity shown as curve TI in the figure, mark the start of wake-induced transition. The changes occur when disturbances in the convecting rotor wake penetrate into the laminar boundary layer of region A and initiate turbulent spots. The streamwise location of transition onset coincides with the small region of local diffusion near 35 percent SSL in Fig. 7b.

This transitional flow appears convecting in time as wake-induced transitional strip B in the s-t diagrams in Figs. 28a and b. For this nozzle, the strip extends from 32 to 80 percent SSL. There is clear definition of both the leading boundary of region B, which lies between points 9 and 4 in Figs. 28a and b, and the trailing boundary between 4 and 10. The leading and trailing boundary velocities of the strip are inferred from the figure to be about 0.9 V_∞ and 0.5 V_∞, respectively. The trajectories for these two convection velocities form the boundaries of region B. These velocities are consistent with the propagation rates of the leading and trailing boundaries of turbulent spots observed by other researchers. Outside the boundary layer the wake convects at the freestream velocity 1.0 V_∞ which in Fig. 28a is greater than (i.e., leads) the leading boundary of strip B.

The evidence that region B is a transitional strip is virtually identical to that for the compressor discussed in Section 7.1 of Part 2.

- The variation of skew along trajectory W in Figs. 28b and e is typical of transition. The skew increases from zero at point 3 (32 percent SSL) marking transition onset. It reaches a positive maximum at 4 (45 percent SSL) and decreases to zero around 5 (55 percent SSL) where intermittency is 0.5. A negative minimum occurs near 6 (65 percent SSL) where intermittency is inferred to be about 0.75. Skew increases to zero by 7 (80 percent SSL) upon completion of transition where intermittency is about one.
- The pattern of random unsteadiness in Figs. 28a and d is also characteristic of transition. The unsteadiness increases along 3–4, indicating transition onset, reaches a maximum (red) at 5, and subsequently decreases in amplitude along 5–6–7 as transition is completed. By 7 the levels are at those seen in the turbulent (green-blue) regions of the boundary layer on this airfoil. Peak random unsteadiness occurs at point 5 in Fig. 28a where skew is zero in Fig. 28b, indicating intermittency $\gamma \approx 0.50$. This is the midpoint of transition. Comparing red trajectories in Figs. 28d and e shows these details in line plots.
- The boundary layer surveys and raw traces are indicative of transition as discussed in Sections 12.3 and 12.4 below.

The discovery that these strips are transitional in nature and not turbulent means that the process of wake-induced transition does not immediately produce a fully turbulent strip with an intermittency of one, as assumed by some researchers.

Wake-Induced Turbulent Strip (C). When transition is complete, the wake-induced transitional strip B becomes a wake-induced turbulent strip identified as region C in Figs. 28a and b. Region C extends along points 7–8 from 80 percent SSL to the trailing edge of the airfoil. Random unsteadiness has decreased to the lower relative levels seen as the blue color in Fig. 28a, and the skew has returned to zero in Fig. 28b. This indicates the transition process had been completed and the boundary layer is turbulent. Convective velocities associated with the leading and trailing boundaries of turbulent strip C were found to be 0.9 V_∞ and 0.5 V_∞, respectively.

12.2 The Path Between Wakes

The development of the boundary layer is now described along the path between wakes. This path begins at the leading edge, goes through point 1 in laminar region A, continues through the laminar region to also include the calmed region, and then goes through the transition and turbulent regions between wakes, E and F, respectively, as it continues to the trailing edge.

The Laminar Region (A). The portion of laminar region A that is of interest here occupies most of the wake passing period. It lies between the rotor wakes where the laminar boundary layer is subjected only to disturbances from other than the

upstream rotor wakes. This portion extends from the leading edge near points 1 to about 50 percent SSL. It is identified by low levels of random unsteadiness (blue area in Fig. 28a), zero skew (blue/green area in Fig. 28b) and decreasing wall shear stress for trajectories X, Y and Z in Fig. 28c.

The Calmed Region (D). As described in Section 4.2 and associated Fig. 9 of Part 1, the turbulent spots produced within wake-induced transitional strip B generate a calmed region that follows the transitional strip in time. This calmed region appears in the path between wakes as region D in Figs. 28a and b. Region D is characterized by low random unsteadiness, near zero skew and elevated levels of shear stress.

Although there is no visual evidence that allows us to identify the calmed region from the ensemble-average results presented in Figs. 28a and b, its existence will clearly be seen in the raw data. The boundary of region D is obtained from raw data traces as the limit where the high shear relaxes asymptotically to low-shear values. This boundary for our data lies along a trajectory of about 0.35 V_∞, which is marked as the dotted line in Figs. 28a and b. Since the relaxation is asymptotic and the appearance of turbulent spots is random, the boundary has some uncertainty.

By comparing the size of the compressor's calmed region D in Fig. 13a with that of the turbine's in Fig. 28a, one can see the calmed region for the turbine is considerably less extensive. As discussed in Section 5.1 of Part 1, this results from differences in time scales based on boundary layer thickness and differences in reduced frequency, which for the turbine is about one-half that for the compressor. As a result, turbulent spots and associated calmed regions have, in a relative sense, less time to grow as they convect along the turbine nozzle in comparison to the compressor stator. Consequently, the transitional behavior between wakes for most of the turbine passage is affected primarily by the level of freestream turbulence entering the nozzle.

How effective is this particular calmed region in Fig. 28a? We reason that the effectiveness of the calmed region in suppressing flow separation and transition onset between wakes is a function of the level of intermittency within the transitional strip and the extent of the calmed region between wakes. As described in Section 11.2, intermittency levels can be inferred from the skew distributions. For this case, the location of 0.75 intermittency does not occur until about 65 percent SSL, which is well past the region of transition onset between wakes. Consequently we judge the calming effect in region D to be weak.

Transition between Rotor Wakes (E, G). Between wakes, the flow undergoes bypass transition that is induced by disturbances other than those associated with wakes from the rotor immediately upstream. These regions of transitional flow are labeled E and G in Figs. 28a and b. Transition between wakes begins on average at 52 percent SSL, which is 20 percent SSL farther downstream than that for region B. This difference is consistent with the lower levels of turbulence intensity between rotor wakes.

The transition processes in regions E and G are described for the three trajectories X, Y and Z which originate upstream along paths that respectively have turbulence intensities of 2.7, 3.4 and 1.7 percent. Along the path between wakes, there is a clear correlation between the streamwise location of transition onset and the variation of turbulence intensity across a wake passing period.

Trajectory X cuts through the calmed region D and region E just behind transitional strip B. Transition along trajectory X, which is delayed relative to that along trajectory Y, is indicated in Figs. 28b and e by positive/zero/negative/zero skew at points 12, 13, 14 and 15, respectively. The delay in transition onset (appearance of increased random unsteadiness) for trajectory X relative to Y in Figs. 28a and d is caused by the lower level of entering turbulence intensity of 2.7 percent and by the small calmed effect. It is not possible to separate these two causes using the data.

Trajectory Y cuts through the portion of region E along points 17–19 that is most influenced by the higher turbulence levels. The calmed region has no influence along this trajectory. The variation in random unsteadiness and the cycle of skew in Figs. 28a, b, d and e is typical of the transition picture described previously.

Trajectory Z, cutting through region G along points 20–22, has the lowest inlet turbulence intensity of 1.7 percent. Region G results from the low level of inlet turbulence intensity and the calming effects following turbulent spots formed in region E. Transition onset along Z occurs at point 20 near 60 percent SSL. The variation in random unsteadiness and skew in Figs. 28d and e clearly show transition is not completed before the trailing edge. On an instantaneous basis, the raw data will show nonturbulent calmed flow extending to the trailing edge of the nozzle for up to 40 percent of the wake passing events.

Turbulent Region Between Wakes (F). The region of turbulent boundary layer downstream of the flow that undergoes transition between wakes is labeled F in Figs. 28a and b. The fluctuations in shear stress at point 16 are similar to that at point 8. The random unsteadiness in region F is lower than that for the transitional flow in region E but higher than that for the laminar flow in region A. The skew is near zero.

The boundaries between regions C and F from about 80 percent SSL to the trailing edge cannot be readily distinguished from the random unsteadiness and skew. However, they can be distinguished in the boundary layer surveys. Higher random unsteadiness in region G can be distinguished around point 22, where calmed regions intermittently reach the trailing edge.

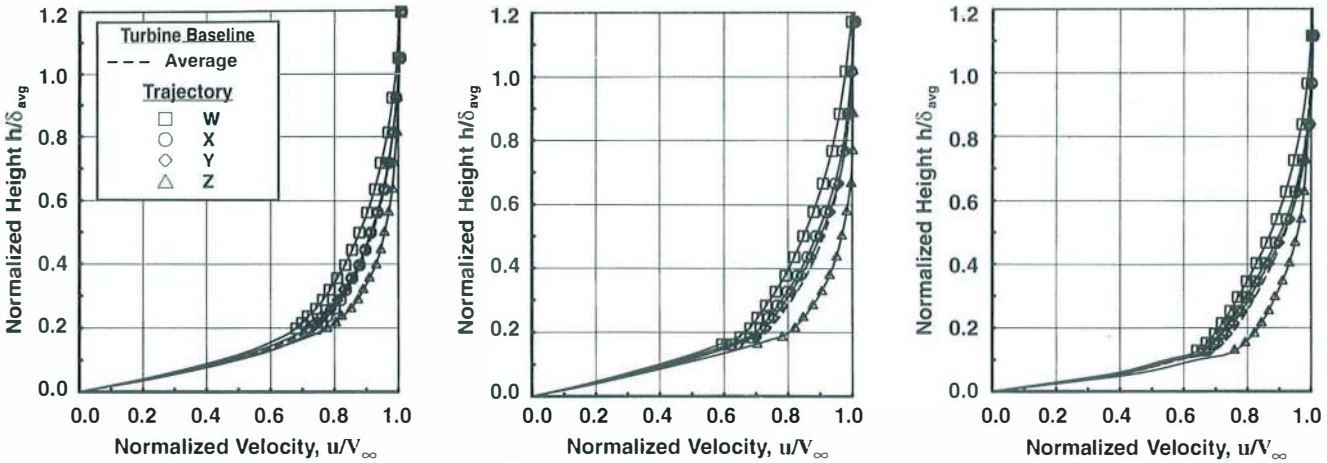

a) 50 percent SSL b) 68 percent SSL c) 82 percent SSL

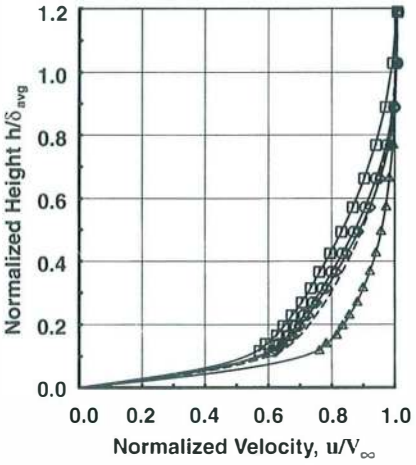

d) 94 percent SSL

Fig. 29 Boundary layer profiles for turbine baseline along Trajectories W, X, Y, and Z in Fig. 28a. Suction surface of second-stage nozzle, profiles normalized by time-average boundary layer thickness, Re = 5.27 x 10^5, Test Point 5A.

12.3 Boundary Layer Surveys

The results presented so far show only what is happening on the airfoil surface. Additional understanding of the state of the boundary layer was achieved by also studying the boundary layer profiles.

Surveys of the boundary layer were obtained at midspan along the nozzle suction surface at streamwise locations of 50, 68, 82 and 94 percent SSL. Boundary layer profiles for Trajectories W, X, Y and Z of Fig. 28a are presented in Figs. 29a–d. The time-averaged profile is shown as a dashed line. Height above the nozzle surface is normalized by the time-averaged boundary layer thickness measured at the given streamwise location instead of the local time-varying value. This allows the thickness of the various boundary layers to be distinguished. Velocity is normalized by the local freestream value of each individual profile. Curve fits of the data were done systematically using a spline fit with weighted averaging and zero velocity imposed at the wall. No custom-tailoring was employed. However, since the turbine boundary layers were very thin (less than 0.8 mm or 0.030 in. at 50 percent SSL), measurements on a normalized basis could not be made as close to the wall as those for the compressor. As a result, there is greater uncertainty in the values of the integral parameters computed using the curve fits of the profiles. This uncertainty decreases with Reynolds number as the boundary layer thickens. Due to the high camber of the turbine nozzle, surveys upstream of 50 percent SSL could not be made.

Ensemble-averaged distributions of the boundary layer integral parameters, obtained by integration of the profile curve fits, are given in Figs. 30a–d for one wake passing period. Displacement and momentum thicknesses are normalized by nozzle suction surface length. Time-averaged values are provided along the right-hand side of each figure.

Profile Shapes. For the predominantly favorable pressure gradient of the turbine, there is only a small distinction between the velocity profiles for wake-induced trajectory W and those for trajectories X and Y in Figs. 29a–d. This is in contrast to the findings for the compressor in Fig. 15, where in the presence of an adverse pressure gradient, the profile for trajectory W was clearly thicker than the others and of a different character.

However, the turbine profile for trajectory Z in Figs. 29a–d is clearly distinguished from the others. This trajectory cuts through region G which is perturbed by the low inlet turbulence and exhibits calmed effects. The boundary layer along trajectory Z is still transitional at the trailing edge and is noticeably thinner than the others.

Integral Parameters. There are two major messages obtained from the integral parameters in Fig. 30. First, the maximum values occur along the wake-induced path W and the minimum values occur along trajectory Z. This is consistent with transition starting farther upstream along W.

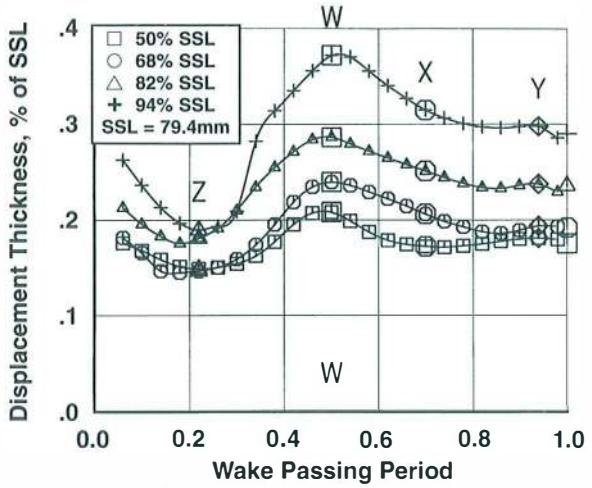

a) Displacement thickness

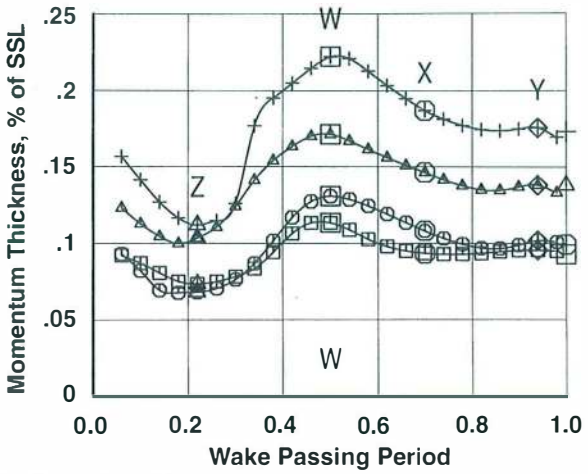

b) Momentum thickness

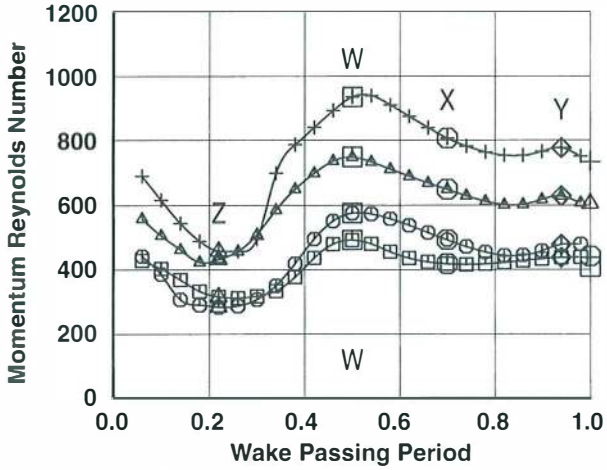

c) Momentum Reynolds number

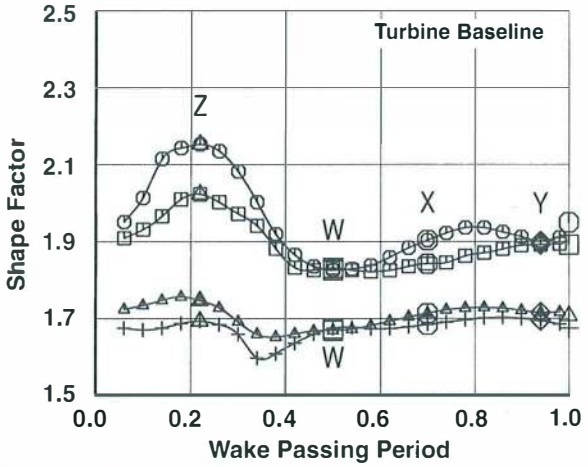

d) Shape factor

Fig. 30 Variation of integral boundary layer parameters across wake-passing period for turbine baseline, suction surface second-stage nozzle. Trajectories W, X, Y, and Z from Fig. 28a are identified. Re = 5.27 x 10^5, Test Point 5A.

Secondly, all values of shape factor are consistent with attached flow.

The nonsymmetrical distributions of displacement and momentum thickness around trajectory W in Figs. 30a and b are noteworthy. The values of each parameter are significantly lower along trajectory Z ahead of the wake-induced strip than they are along trajectories X and Y behind it. This is likely due to the long streamwise extent of transitional flow in region G along trajectory Z.

12.4 Analysis of Raw Data

The raw data are examined because they show evidence for important flow features, such as the calmed effect and velocities of individual turbulent spots, that cannot be seen in ensemble-averaged data.

Instantaneous time traces of quasi wall shear stress, presented in A-C coupled format, are shown in Fig. 31 for the suction surface of the second-stage nozzle. The traces were obtained simultaneously. Trajectories W through successive wake passing periods are given numerical subscripts. Areas of importance are encircled and identified with a number.

The Laminar Region A. Time traces for the perturbed laminar region A of Fig. 28a extend along the first 25 percent of the airfoil in Fig. 31. Traces near the leading edge contain only low amplitude fluctuations indicative of a laminar boundary layer. At 25 percent SSL, stronger periodic variations associated with the jet-wake effect, which in turbines transports rotor wake fluid towards the nozzle suction surface, are evident as illustrated by encircled area 1. The ensemble-mean distributions, superimposed on the figure as dashed lines at 25 and 32 percent SSL, further illustrate the periodic

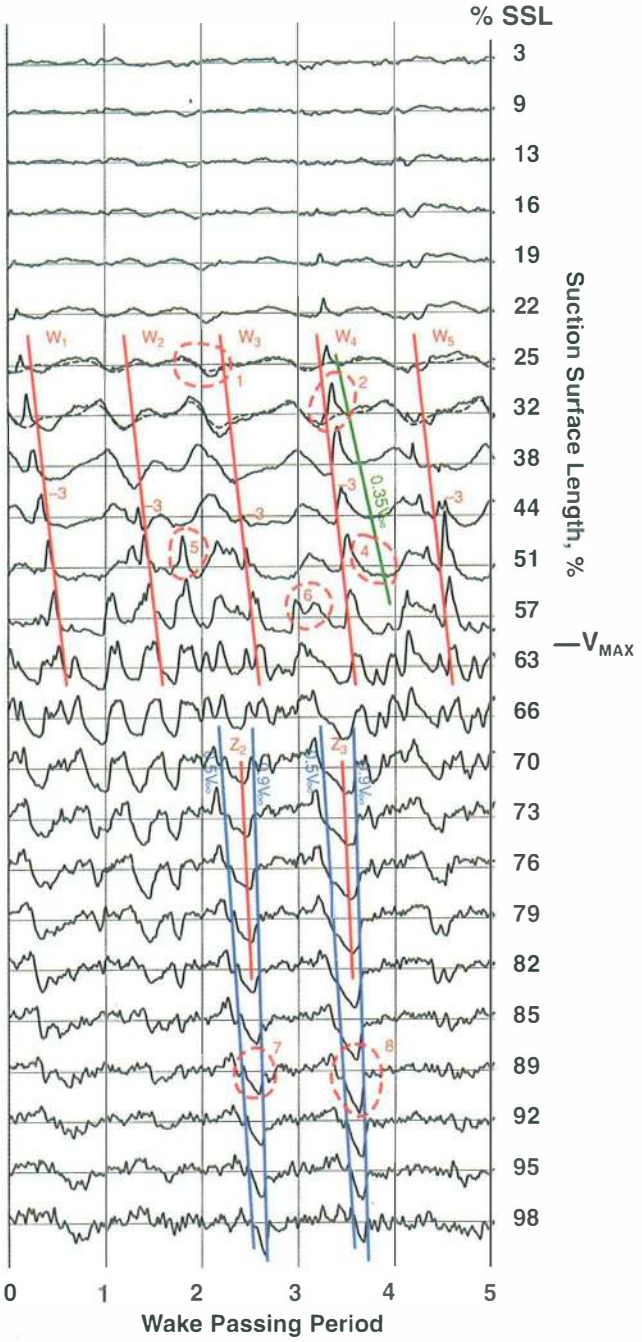

Fig. 31 Raw time traces from surface hot-film gauges operated simultaneously on the suction surface of second-stage nozzle N2, Turbine Test Point 5A.

nature of this jet-wake effect. Characteristics of jet-wake interaction that would produce these features were documented by Hodson (1984).

Wake-Induced Transitional Strip B. Wake-induced transition is clearly underway by 32 percent SSL. Turbulent spots originate in the vicinity of the W trajectories such as those shown along W_4 in area 2. The time period between succes-

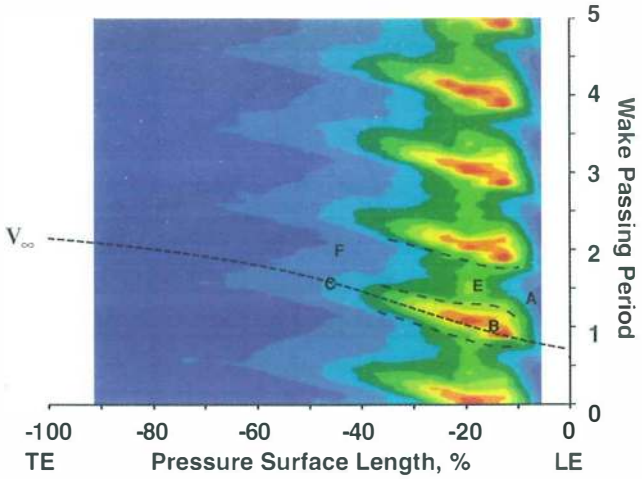

Random Unsteadiness Q_0 = 1.29, Q_{10} = 19.1

Fig. 32 Shear stress characteristics on pressure surface of second stage nozzle, Re = 1.80 x 10^5, turbine baseline, test point 5D

sive spots does not correlate as closely with wake passing as that seen for the compressor. Instead, spots both lead and lag the equally spaced W trajectories. Convection velocities appear to vary as well. The average convection velocities of the spots along W_1 and W_2 are somewhat less than 0.7 V_∞ while those along W_4 and W_5 are somewhat greater. At 44 percent SSL, turbulent events of varying amplitude occur for each passing wake as seen by the various magnitudes of marker "3" in the figure.

Calmed Region D. The calmed regions are identified in Fig. 31 as areas of elevated but decaying shear stress following turbulent spots. An example is seen as area 4. The downstream boundary of the region is determined by locating where flow breakdown occurs and constructing a trajectory from the origin of the strip to the breakdown point. The green trajectory of 0.35 V_∞ is an example. The average temporal extent of the turbulent spots and the associated calmed regions are significantly less than those for the compressor as described previously in Section 12.2.

Transition Between Wakes E. The onset of transition between the wake-induced strips takes place near 50 percent SSL prior to maximum velocity. Single-spot events in area 5 and multiple-spot events in area 6 mark transition onset in Fig. 31. The relative locations of the spots between wake events coincide with the regions of elevated freestream turbulence described previously in the introduction of Section 12.0. The presence of numerous spots at 63 percent SSL makes it impossible, in general, to distinguish the wake from the non-wake-induced areas at this location. Downstream of maximum velocity, the turbulent events continue to engulf the remaining laminar flow. By 85 percent SSL, transition is nearly complete.

Along trajectories Z_2 and Z_3 which begin at 70 percent SSL in Fig. 31, areas of calmed flow persist all the way back to the trailing edge, as illustrated by areas 7 and 8. Due to their elevated levels of shear stress, these areas of nonturbulent boundary layer do not separate even in the presence of the mild adverse pressure gradient in this region. As expected, these events coincide with region G in Fig. 28a.

No evidence of T-S waves was found. Rather, the flow in the region between wakes undergoes bypass transition.

12.5 The Pressure Surface

The boundary layer development along the pressure surface is shown for Test Point 5D in Fig. 32. These measurements are presented at the cruise $\overline{Re} = 1.80 \times 10^5$ for consistency with a later comparison. However, results along the pressure surface were found not to vary appreciably with Reynolds number.

A short region of laminar boundary layer exists from the leading edge to about 10 percent PSL. This appears as the blue color and is marked region A. Transition, which begins near the leading edge in the region of adverse pressure gradient is completed relatively quickly compared to that on the suction surface.

For the wake path, transition occurs in a wake-induced transitional strip shown by the red-orange-yellow region B. Transition begins at about 10 percent PSL and is completed by about 40 percent PSL. The skew (not shown) has a general appearance of transition but it is less pronounced than that for the suction surface. Following region B, there is a turbulent boundary layer marked C, which remains attached until the trailing edge.

Between wakes, transition occurs in the strong adverse pressure gradient from about 12 to 30 percent PSL in region E. The turbulent boundary layer F, which follows from region E, remains attached to the trailing edge.

13.0 REYNOLDS NUMBER EFFECTS ON TURBINE BOUNDARY LAYERS

This section examines the influence of Reynolds number on LP turbine boundary layers. It provides the evidence for Fig. 10d in the discussion in Section 5.0. It shows that as Reynolds number is reduced from the high values at take-off to low values at cruise, the wake-induced transitional strips weaken and move toward the trailing edge. The location of transition onset between wakes also moves toward the trailing edge. This conclusion was similar to that for compressors. The turbine findings are evaluated relative to those for the baseline in Section 12.0. The results are listed in Table 6.

The Reynolds number tests for the embedded second stage of the LP turbine were conducted at stage-average Reynolds numbers of 5.27×10^5, 3.96×10^5, and 2.71×10^5 for take-off conditions and 1.80×10^5 and 1.19×10^5 for cruise conditions. These are test points 5A, 5B, 5C, 5D and 5E, respectively.

13.1 Picture Constructed from Surface Film Data

Cruise (Low) Reynolds Numbers. The s-t diagram of random unsteadiness for the cruise (low) Reynolds number of 1.19×10^5 is shown in Fig. 33a. This flow picture is markedly different from that at the high (baseline) Reynolds number shown in Fig. 28, and in abbreviated form in Fig. 33b.

The striking feature of Fig. 33a is the very great extent of laminar region A and the near absence of wake-induced transitional strips penetrating this laminar region. The favorable pressure gradient for this airfoil extends to about 62 percent SSL, as seen in Fig. 7b. Transition onset does not occur until 73 percent SSL along the wake-influenced trajectory W. This is well into the region of mild diffusion. The subsequent wake-induced region is labeled B in the figure. Between wakes, a significant calmed region D develops which inhibits flow separation. However, some evidence of transition between wakes, denoted by region E, is present as well. Transition in both regions B and E extends to the trailing edge. Even at this low Reynolds number, no flow separation was observed. The results for the cruise $\overline{Re} = 1.80 \times 10^5$ were similar.

Take-off (Higher) Reynolds Numbers. The s-t diagrams of random unsteadiness for take-off $\overline{Re} = 2.70 \times 10^5$ and 5.27×10^5 are shown in Fig. 33b. As Reynolds number is increased from cruise values through the take-off range, Figs. 33a and b show quite a compelling picture of transition as regions B, C, D, E and F move progressively upstream and become more defined. Transition onset for the wake-induced strips moves from 73 to 71 to 48 to 34 to 32 percent SSL as Reynolds number is progressively increased. (Not all of these data are shown.) At take-off Reynolds numbers, transition onset is influenced by the short region of slight adverse pressure gradient near 35 percent SSL in Fig. 7b. The beginning of transition between wakes moves from 80 to 76 to 60 to 52 to 52 percent SSL. For $\overline{Re} = 2.70 \times 10^5$ in the upper region of Fig. 33b, the high levels of random unsteadiness at the trailing edge indicate that transition along both the wake and nonwake paths has not yet been completed.

At take-off Reynolds numbers, the calmed effect has much less impact on the transition process for turbines than it has for compressors and transition is tied more closely to the level and variation of freestream turbulence entering the blading. For cruise Reynolds numbers, however, calmed effects played an important role in suppressing laminar separation.

Quasi Wall Shear Stress. Distributions of quasi wall shear stress for the various Reynolds numbers are shown in Fig. 34. For the two cruise Reynolds numbers (Test Points 5D and 5E), the shear stress continues to decrease in a manner characteristic of laminar boundary layers until the onset of transition at about 80–90 percent SSL. For $\overline{Re} = 1.80 \times 10^5$, shear stress along all of the trajectories W through Z exhibit the same features.

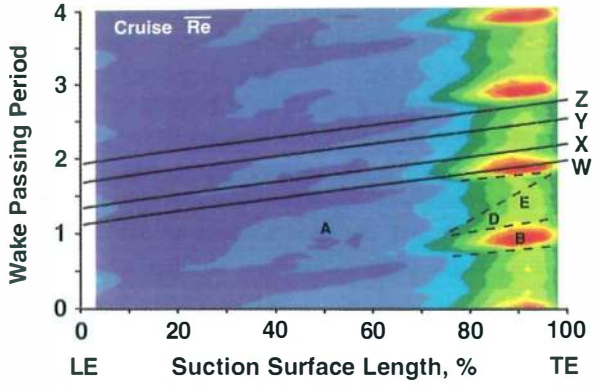

a) Cruise $\overline{Re}$ = 1.19x10^5, Test Point 5E, Q_0 = 1.13, Q_{10} = 23.73

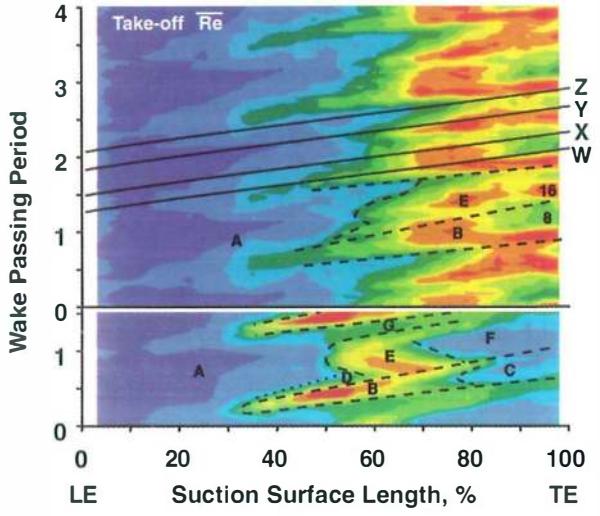

b) Take-off, (upper portion) $\overline{Re}$ = 2.7 x 10^5, Test Point 5C, Q_0 = 1.20, Q_{10} = 11.20 (lower portion) $\overline{Re}$ = 5.27 x 10^5, Test Point 5A, from Fig. 28

Fig. 33 Reynolds number effect on boundary layer development. Suction surface, turbine nozzle N2. Data shown as s-t diagrams of random unsteadiness.

For the higher Reynolds numbers, average shear stress in Fig. 34 begins to increase between 40 and 50 percent SSL indicating transition onset occurring much earlier than at cruise values.

13.2 Boundary Layer Surveys

Surveys of the boundary layer were obtained for the cruise (low) $\overline{Re}$ = 1.80 x 10^5 at the same locations as those for the take-off Reynolds number shown in Fig. 29. Compared to the profiles for the take-off Reynolds numbers, the profiles for the cruise Reynolds numbers (not shown) are less full. Profiles W and X at 50 percent SSL are clearly laminar. Trajectories W through Z take on a transitional character as one moves toward the trailing edge.

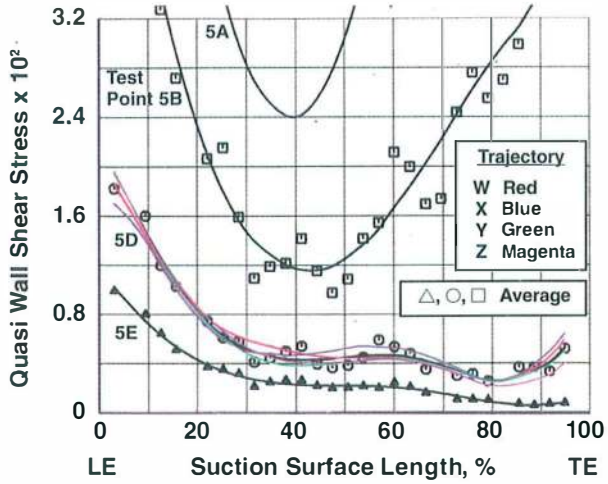

Fig. 34 Reynolds number effect on quasi wall shear stress. Suction surface, turbine nozzle N2. Time-average values shown for Test Points 5A from Fig. 28c, 5B, 5D and 5E. Trajectories W, X, Y and Z also shown for Test Point 5D.

The integral parameters, shown in Fig. 35, have a somewhat different character than those in Fig. 30. The distributions about W are now more symmetrical at cruise than they are at take-off. The lower values associated with region G along trajectory Z at take-off are not present at cruise since transition everywhere has moved well aft on the airfoil. At cruise Reynolds number the boundary layers are thicker, as expected, with maximum values lying under the wake-disturbed region W. The maximum-to-minimum ratios of both displacement thickness and momentum Reynolds number in Fig. 35 are about 1.4 compared to a value of about 2.0 for the take-off Reynolds number in Fig. 30.

Values of shape factor vary between 2 and 2.6 at cruise Reynolds numbers, indicating that no flow separation occurred. These values are somewhat higher than those for take-off conditions.

13.3 Analysis of Raw Data for Cruise Reynolds Number

An abbreviated set of instantaneous time traces (raw data) of quasi wall shear stress for the cruise Reynolds number of 1.19 x 10^5, Test Point 5E, are shown in Fig. 36. The most striking feature of these traces is the absence of any transitional flow along the first three quarters of the nozzle suction surface. In contrast, wake-induced transition occurred as early as 30 percent SSL for the baseline test case as shown in Fig. 31.

For cruise Reynolds numbers, wake-induced transition is not evident until 79 percent SSL, as noted from the turbulent events labeled "1" in Fig. 36. Distinct calmed regions, examples of which are labeled "2" for various streamwise locations, develop behind the wake-induced events as they convect downstream. This calming effect produces elevated levels of nonturbulent shear stress between the turbulent events.

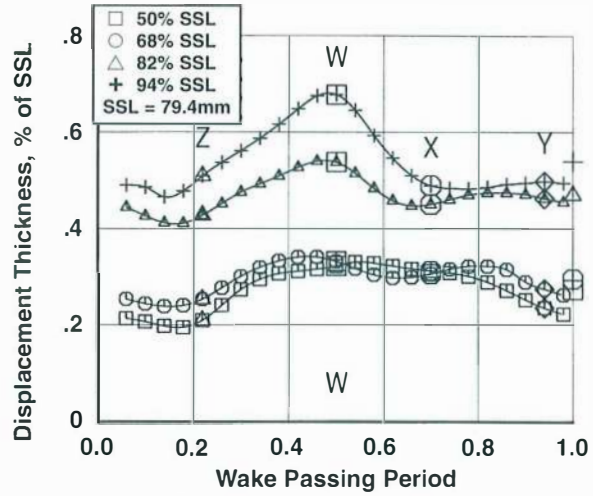

a) Displacement thickness

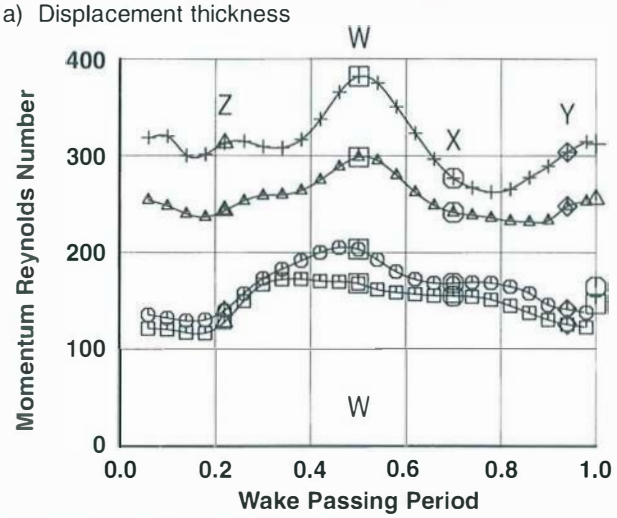

b) Momentum Reynolds number

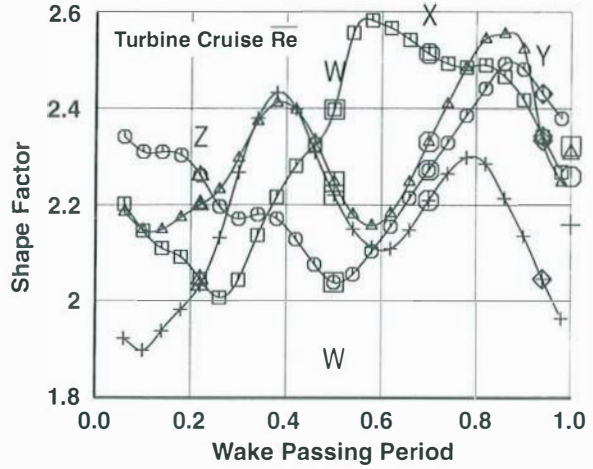

c) Shape factor

Fig. 35 Variation of integral boundary layer parameters across wake-passing period for Turbine cruise Reynolds number, suction surface of the second-stage nozzle. $\overline{Re}$ = 1.80 x 10^5, Test Point 5D.

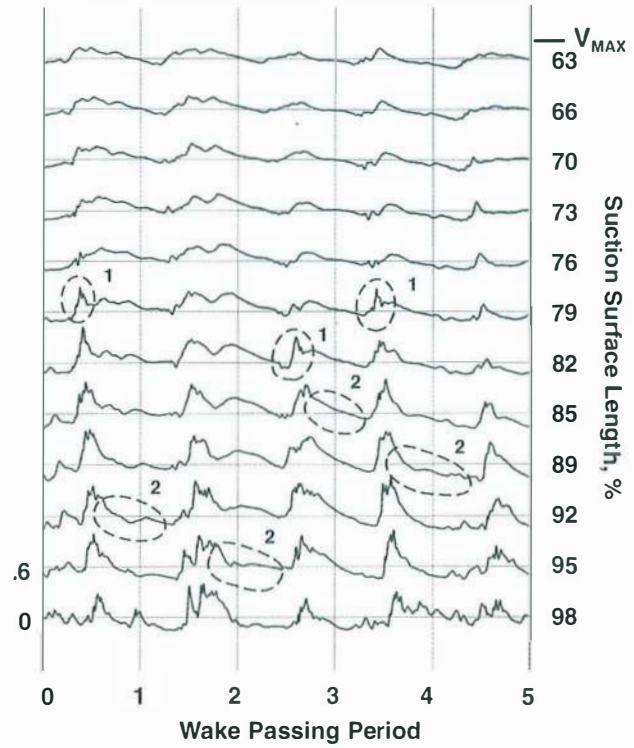

Fig. 36 Instantaneous time traces (raw data) from surface hot-film gauges for turbine curise Reynolds number. Gauges operated simultaneously. Suction surface of second-stage nozzle, $\overline{Re}$ = 1.19 x 10^5, Test Point 5E

The asymptotically decreasing wall shear through the above-mentioned calmed regions indicates that the boundary layer between wake-induced strips remains attached. This is especially evident when the calmed effect is strong.

Instantaneous time traces obtained at the higher cruise Reynolds number of 1.80 x 10^5 (Test Point 5D) contained identical features to those described above. Values of shape factor from this latter test condition in Fig. 35c provide further evidence that no flow separation of the nonturbulent flow occurs prior to the trailing edge in spite of the mild adverse pressure gradient. This is in contrast to conventional boundary layer calculations which predict laminar separation to occur prior to 80 percent SSL for this blading. This feature will be discussed in Part 4.

At 98 percent SSL, significant regions of nonturbulent flow persist. An intermittency level of only about 0.6–0.7 was inferred visually from numerous traces at this trailing-edge location.

14.0 LOADING EFFECTS ON BOUNDARY LAYERS

This section examines the influence of airfoil loading on boundary layer development for embedded stages of LP turbines. It provides the evidence for Fig. 10f of the discussion in Section 5.0. It shows that decreasing the loading weakens

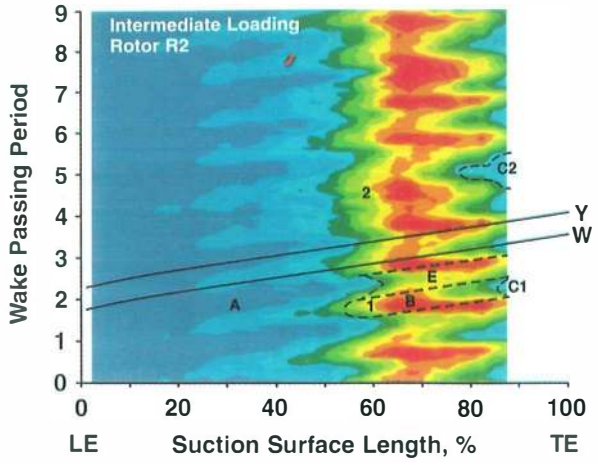

a) Random unsteadiness, $Q_0 = 0.83$, $Q_{10} = 13.23$

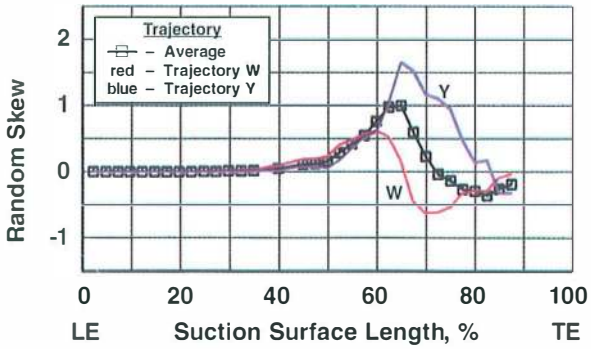

b) Skew

Fig. 37 Loading effect on rotor boundary layer development. Suction surface, turbine rotor R2. Intermediate Loading, Test Point 6A.

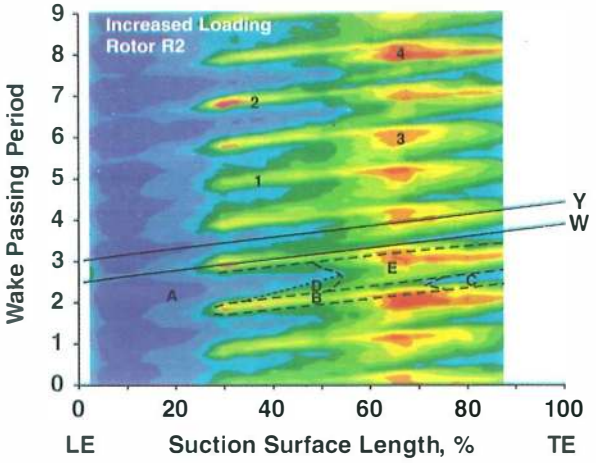

a) Random unsteadiness, $Q_0 = 0.69$, $Q_{10} = 11.99$

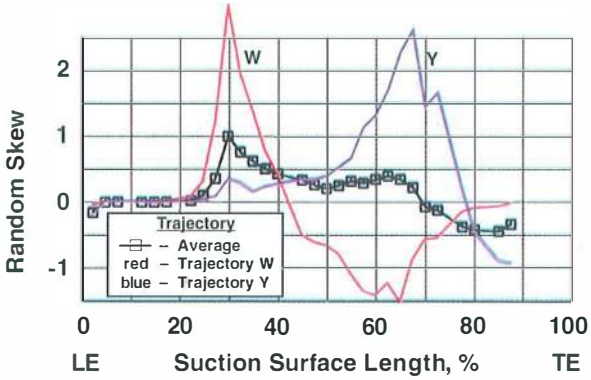

b) Skew

Fig. 38 Loading effect on rotor boundary layer development. Suction surface, turbine rotor R2. Increased Loading, Test Point 5B.

the wake-induced transitional strips as they move downstream. The findings are evaluated relative to those for the baseline. The results are listed in Table 6.

14.1 Loading Effects for the Suction Surface

Loading effects were evaluated systematically for the embedded second stage of the LP turbine. Since the results for the rotor and nozzle were similar, we chose to show the rotor results because they illustrate the additional feature of "beating" as described below. S-t diagrams of random unsteadiness are presented for intermediate and increased loading, Test Points 6A and 5B, respectively. For intermediate loading, it is important to note from Fig. 7a that a continuous flow acceleration was maintained from the leading edge to maximum velocity. In contrast, at increased loading, a region of local diffusion occurs near 25 percent SSL. Data for Test Point 6A were obtained at design RPM. The Reynolds number is about 15 percent greater than that for Test Point 5B. However, based on the results just presented in Section 13.1, this difference is not significant.

The shear stress characteristics for the turbine rotor R2 at intermediate loading Test Point 6A are presented in Fig. 37. The random unsteadiness in Fig. 37a shows a large extent of laminar region A. Wake-induced transition in region B does not begin until about 50 percent SSL. A small region of turbulent boundary layer, C1, follows region B near the trailing edge. Between wakes, transition begins in region E and the flow between wakes remains transitional at the trailing edge.

The difference in the transitional character of regions B and E is seen by comparing the skew for trajectories W and Y in Fig. 37b. Wake-induced trajectory W has completed the zero-positive-zero-negative-zero transition cycle of skew while trajectory Y has only completed about half of the cycle, even though the two trajectories begin their initial rise at about the same percent SSL.

At increased rotor loading in Fig. 38a, the wake-induced strips B now begin at about 25 percent SSL near the location of local diffusion. Transition between wakes in region E moves upstream to about 53 percent SSL. The skew for tra-

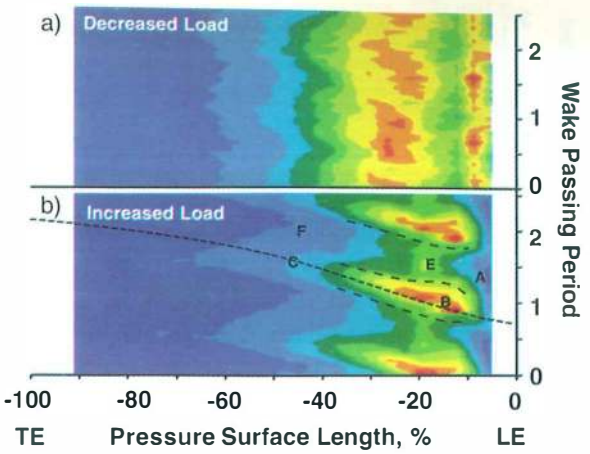

Fig. 39 Loading effect on boundary layer development. Pressure surface, turbine nozzle N2, s-t diagram of random unsteadiness. a) Decreased loading Test Point 7B, $Q_0 = 2.37$, $Q_{10} = 17.57$. b) Increased Loading Test Point 5D, $Q_0 = 1.29$, $Q_{10} = 19.09$

jectory W in Fig. 38b begins its cycle at about 25 percent SSL, well ahead of that for trajectory Y between wakes. Transition for trajectory W is complete by 75–80 percent SSL while it is only just over half complete for trajectory Y between wakes.

An additional feature of the wake-passing events in the rotor s-t diagrams of Figs. 37a and 38a is the "beating" pattern which occurs at the frequency difference associated with the differing vane count. Nozzle N1 has 82 airfoils while Nozzle N2 has 108 airfoils. Consequently, the N1/N2 orientation varies with circumferential position. This causes a beating effect on boundary layer development as can be seen by comparing the wake-induced strips at points 1 and 2 in each of the figures. Behind point 2 in Fig. 37a, where the interaction is stronger, transition is completed sooner and the region of turbulent boundary layer at C2 is larger than that at C1 where the interaction is weaker. In Fig. 38a this effect can also be seen by comparing points 3 and 4 between wakes.

14.2 Loading Effects for Pressure Surface

We return to the nozzle results to evaluate the effect of loading on boundary layer development along the pressure surface. At decreased loading in Fig. 39a (Test Point 7B), the high negative incidence and strong adverse pressure gradient near the leading edge (see Fig. 7) cause flow separation at the leading edge with reattachment at about 5 to 8 percent PSL. At increased loading in Fig. 39b, the high incidence allows the flow to remain attached as described previously in Section 12.5.

15.0 NOZZLE-NOZZLE INTERACTION (CLOCKING EFFECTS)

This section examines the effect that clocking nozzle N1 relative to nozzle N2 has on boundary layer development on embedded nozzle N2. It provides the evidence for Fig. 10h of the discussion in Section 5.0. It shows clocking effects can produce quite different boundary layers on the suction surfaces of the LP blading.

15.1 Wake Interaction

Significant wake interaction (dispersion) occurs in a LP turbine as upstream nozzle wakes convect through the downstream rotor (Arndt, 1993). This situation is illustrated in Fig. 40a, which shows the upstream nozzle wakes (lightly shaded regions in the figure) being stretched and turned as they convect through the following rotor. Instrumentation placed at the measurement plane shown downstream of the rotor in the figure will detect both the rotor wakes and the dispersed wake segments of the nozzle. This combined wake signature will vary depending upon the circumferential position of the instrumentation relative to the upstream nozzle.

Figure 40a relates to our test configuration in that the upstream nozzle is nozzle N1 and the rotor is rotor R1 as seen in Fig. 4. Two clocking examples are illustrated by the two parallel arrows shown in Fig. 40a; one arrow is located at 60 percent relative N1 pitch, and the other at 20 percent relative pitch. The arrows show the absolute flow direction the wakes take past a stationary probe placed at each of the two clocking positions. The rotor in Fig. 40a is shown frozen at an instant in time. If one allows the "film to roll" (i.e., the rotor to rotate), specific wake features, identified by the numbers adjacent to each arrow, will convect past the stationary instrumentation in the absolute frame (i.e., along the arrow). This unsteadiness pattern will be felt by our downstream nozzle N2.

As the wakes convect past the 60 percent relative N1 pitch location in Fig. 40a, the instrumentation (and nozzle N2 when aligned with the arrow) will see a turbulence intensity pattern as measured along absolute flow trajectory 1-2-3-4 marked in the figure. The number "2" identifies the peak TI within the R1 wake and "4" denotes the peak TI within the N1 wake segment. This measured pattern of turbulence intensity is shown in Fig. 40b. Similarly at 20 percent relative N1 position in Fig. 40a, the TI pattern follows along 5-6-7-8, with the measured values shown in Fig. 40c. For reference, all nozzle results presented up to this point were obtained with nozzle N1 at 40 percent relative pitch to nozzle N2. The turbulence pattern for this orientation is superimposed onto Fig. 28a.

15.2 Effect of Nozzle Clocking on the Boundary Layer

The boundary layer development for the two clocking positions described above is shown in Fig. 41. The numbers superimposed on the figures correspond to those in Fig. 40 which identify various levels of turbulence intensity. As observed previously, transition onset at each numbered location in Fig. 41 follows closely the variation in inlet turbulence

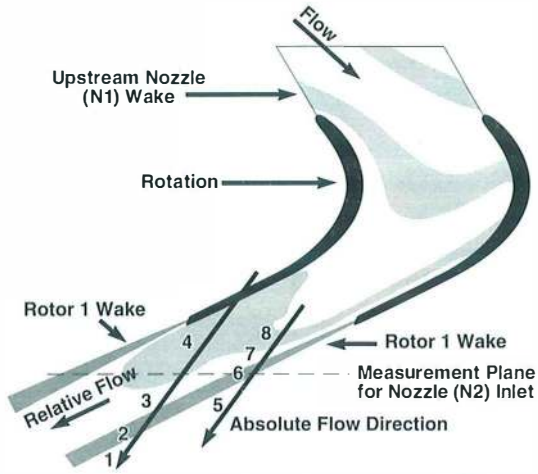

a) Sketch of wake convection (after Denton, 1993).

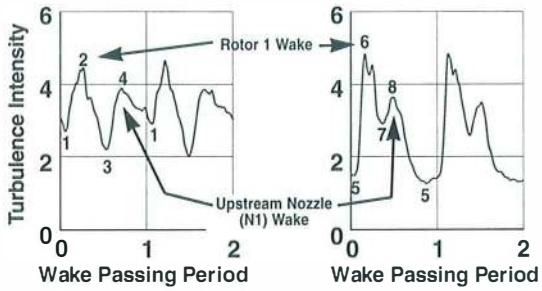

b) 60% relative pitch c) 20% relative pitch

Fig. 40 Wake convection in a multistage LP turbine.

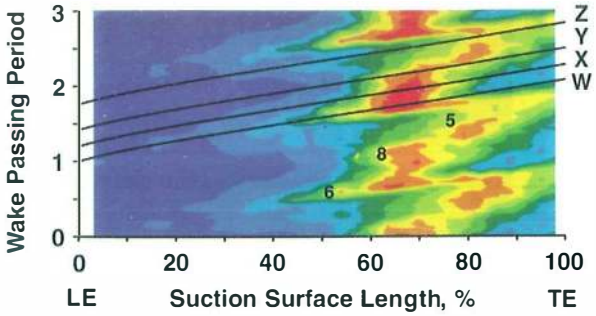

a) 20 Percent relative N1 pitch, $Q_0 = 0.56$, $Q_{1C} = 9.66$

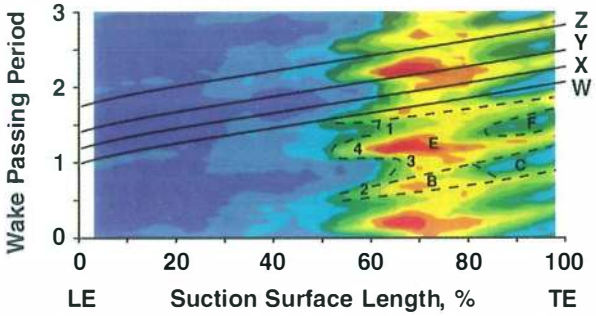

b) 60 Percent relative N1 pitch, $Q_0 = 0.56$, $Q_{1C} = 9.66$

Fig. 41 Effect of Nozzle one (N1) clocking on boundary layer development along Nozzle Two (N2). Turbine suction surface. Test Point 6A.

Table 6 Effect of Reynolds number and loading on boundary layer development for turbines. Tabulated numbers give locations of regions along suction surface of airfoil in percent SSL.

REGION	$\overline{Re} \times 10^{-5}$ OR LOADING LEVEL	TEST POINT	A LAMINAR REGION		B WAKE-INDUCED TRANSITIONAL STRIP			C WAKE-INDUCED TURBULENT STRIP		D CALMED REGION	E TRANSITION BETWEEN WAKES			F TURBULENT BETWEEN WAKES	
			L	T_B / T_E	*L*	$0.5\gamma / 0.75\gamma$	*T*	*L*	*T*	*Effective*	*L*	0.5γ	*T*	*L*	*T*
TURBINE NOZZLE	5.27	5A	LE	32/52	32	56/66	80	80	TE	Low	52	62	73	73	TE
	3.96	5B	LE	34/52	34	65/73	83	83	TE	Low	52	66	84	84	TE
	2.71	5C	LE	48/60	48	76/85	93	93	TE	Low	60	82	TE	—	—
	1.80	5D	LE	71/76	71	90/–	TE	—	—	High	76	93	TE	—	—
	1.19	5E	LE	73/80	73	90/–	TE	—	—	High	80	—	TE	—	—
TURBINE ROTOR	Inter-mediate	6A	LE	50/57	50	66/72	84	84	TE	Low	57	84	TE	—	—
	Increased (High)	5B	LE	25/53	25	42/64	80	80	TE	Low	53	78	TE	—	—
TURBINE NOZZLE	Low	7A	LE	52/62	52	70/76	91	91	TE	Low	62	95	TE	—	—
	Increased (High)	5B	LE	34/52	34	65/73	83	83	TE	Low	52	66	84	84	TE

* Separation
L ≡ Leading boundary of region
T ≡ Trailing boundary of region
γ ≡ Intermittency

T_B ≡ Trailing boundary of laminar region along wake-induced transitional strip B (Trajectory W)
T_E ≡ Trailing boundary of laminar region for transition between wakes E (Trajectory Y)

intensity shown by the time-traces in Figs. 40b and c.

The flow picture from Fig. 41a is very similar to that observed for the baseline in Fig. 28. Its periodic variation is primarily at the blade passing frequency. On the other hand, the picture in Fig. 41b, which corresponds to Fig. 10h, shows the development of two distinct transitional/turbulent strips. One is due to the wake of Rotor R1 and the other is due to the wake segment of Nozzle N1. Periodic variations in the boundary layer occur at twice the blade passing frequency at the trailing edge.

These measurements clearly show that *at least two* upstream bladerows are required in test vehicles in order to produce the actual disturbance environment, including the nozzle-nozzle clocking effect, that is present in embedded stages.